RESEARCH

Recombinant Slit2 suppresses neuroinflammation and Cdc42-mediated brain infiltration of peripheral immune cells via Robo1–srGAP1 pathway in a rat model of germinal matrix hemorrhage

Qian Li[1,2], Lei Huang[3,4], Yan Ding[3], Prativa Sherchan[3], Wenjie Peng[1] and John H. Zhang[3,4*]

Abstract

Background Germinal matrix hemorrhage (GMH) is a devastating neonatal stroke, in which neuroinflammation is a critical pathological contributor. Slit2, a secreted extracellular matrix protein, plays a repulsive role in axon guidance and leukocyte chemotaxis via the roundabout1 (Robo1) receptor. This study aimed to explore effects of recombinant Slit2 on neuroinflammation and the underlying mechanism in a rat model of GMH.

Methods GMH was induced by stereotactically infusing 0.3 U of bacterial collagenase into the germinal matrix of 7-day-old Sprague Dawley rats. Recombinant Slit2 or its vehicle was administered intranasally at 1 h after GMH and daily for 3 consecutive days. A decoy receptor recombinant Robo1 was co-administered with recombinant Slit2 after GMH. Slit2 siRNA, srGAP1 siRNA or the scrambled sequences were administered intracerebroventricularly 24 h before GMH. Neurobehavior, brain water content, Western blotting, immunofluorescence staining and Cdc42 activity assays were performed.

Results The endogenous brain Slit2 and Robo1 expressions were increased after GMH. Robo1 was expressed on neuron, astrocytes and infiltrated peripheral immune cells in the brain. Endogenous Slit2 knockdown by Slit2 siRNA exacerbated brain edema and neurological deficits following GMH. Recombinant Slit2 (rSlit2) reduced neurological deficits, proinflammatory cytokines, intercellular adhesion molecules, peripheral immune cell markers, neuronal apoptosis and Cdc42 activity in the brain tissue after GMH. The anti-neuroinflammation effects were reversed by recombinant Robo1 co-administration or srGAP1 siRNA.

Conclusions Recombinant Slit2 reduced neuroinflammation and neuron apoptosis after GMH. Its anti-neuroinflammation effects by suppressing onCdc42-mediated brain peripheral immune cells infiltration was at least in part via Robo1–srGAP1 pathway. These results imply that recombinant Slit2 may have potentials as a therapeutic option for neonatal brain injuries.

Keywords Germinal matrix hemorrhage, Slit2, Robo1–srGAP1, Neuroinflammation, Apoptosis, Rat

*Correspondence:
John H. Zhang
johnzhang3910@yahoo.com
Full list of author information is available at the end of the article

Li *et al. Journal of Neuroinflammation*　　(2023) 20:249

Page 2 of 16

Introduction

Germinal matrix hemorrhage (GMH) occurs while fragile blood vessels are ruptured inside the subependymal brain tissue [1]. Preterm infants are the most vulnerable group suffering from GMH, with approximate 3.5 cases out of every 1000 births. GMH leads to developmental delays, mental retardation, cerebral palsy, and even posthemorrhagic hydrocephalus with devastating effects [1, 2]. There are two levels of brain damage caused by GMH. The primary damage takes place within the first few hours after hemorrhage and is largely due to hematoma formation, which causes mechanical harm to adjoining tissues [3]. Secondary brain damage causes the further neurological deterioration with significant inflammatory responses [4]. As current treatments for GMH-induced primary damage have not shown conclusive benefits in clinical trials yet, vast majority of studies are focusing on secondary damage to find effective therapeutic targets [4–6].

Several studies have shown that pronounced inflammatory responses occur during GMH-induced secondary brain injury [7–9]. Following brain hemorrhage, resident immune cells are activated and release proinflammatory cytokines and chemokines, such as tumor necrosis factor-α (TNF-α) and interleukin 6 (IL-6), inducing endothelial cells to upregulate intercellular adhesion molecule (ICAM-1) [10, 11]. Such proinflammatory signaling also promotes the migration of peripheral immune cells into the brain that further exacerbate neuroinflammation after GMH [12–16].

Slit family are secreted extracellular matrix-associated glycoproteins, which inhibit leukocyte chemotaxis, regulate axon guidance and control neuronal migration. They are expressed endogenously on neurons and astrocytes in the brain [17, 18]. Vascular endothelial cells secrete Slit2 binds to the transmembrane receptor Robo1 on leukocytes and acts as an endogenous inhibitor of leukocyte chemotaxis [17, 19, 20]. The Slit2 signaling has been shown to be protective in experimental models of systemic inflammation [21–23]. The systemic administration of Slit2 inhibited leukocyte migration to cortical venules after the global cerebral ischemia in mice [24].

Slit2 regulates neuron migration by enhancing the interaction between the Robo1 receptor and Slit-RoboGTPase-activating protein 1 (srGAP1), a downstream effector of Slit2/Robo1signaling [25–27]. The small Rho GTPase Cdc42 [28], a critical mediator of cell motility and neuronal guidance, is subsequently inactivated upon the activation of Slit signaling [20, 29–31]. These genes are also expressed in leukocytes[29]. Robo1 was expressed on the surface of peripheral immune cells [26]. Therefore, the Robo1/srGAP1/Cdc42 signal transduction pathway mediates the anti-migratory effect of Slit2, which may attenuate the peripheral immune cells infiltration into the brain.

Our previous studies demonstrated the protective effects of Slit2 on blood brain barrier (BBB) preservation and anti-neuroinflammation in an adult rat model of surgical brain injury [26]. Given the differences in pathophysiology and age population of GMH, the role of Slit2 remains unclear in in the setting of GMH. This study aimed to evaluate the effects of recombinant Slit2 as a potential treatment to minimize neuroinflammation, and to explore potential underlying mechanisms of Robo1/srGAP1 in inhibiting Cdc42-mediated brain infiltration of peripheral immune cells after the experimental GMH.

Materials and methods

All procedures are conducted in accordance with the National Institutes of Health Guidelines for Laboratory Animal Handling and are approved by the Institutional Animal Care and Use Committee at Loma Linda University. A total of 240 Sprague–Dawley rat pups aged of 7 days old (P7) were used in this study. The brain development stage of P7 in a rat is comparable to that of a infant between 30 and 32 weeks of gestation.

Experimental design and groups
Experiment 1
To determine the time course of endogenous brain Slit2 and Robo1 expression following GMH, the P7 rat pups ($n = 42$, 6/group) were randomly divided into five groups: sham, GMH day 1, GMH day 3, GMH day 5, and GMH day 7. Whole brain tissues were used for Western blotting. Additional 12 rats from groups of sham (6/group), GMH day 1 (3/group) and day 5 (3/group) were used for immunofluorescence staining.

Experiment 2
To determine whether knockdown of endogenous Slit2 exacerbated brain edema, thereby worsening short-term neurological deficits after GMH, the P7 rat pups were randomized to the following experimental groups: sham, GMH, GMH+Slit2 siRNA, and GMH+Scramble siRNA. Brain water content ($n = 24$, 6/group) was evaluated at 24 h after GMH. Another set of animals ($n = 24$, 6/group) were used to evaluate the short-term neurological deficits from 1 to 3 days after GMH, after which animals were euthanized for Western blotting on day 5 after GMH.

Experiment 3
The effects of exogenous recombinant Slit2 treatment on GMH were evaluated. Three doses of recombinant Slit2 (1, 3, and 10 µg/kg, R and D Systems, Minneapolis, MN, USA) were tested. Dosage was selected based on the

Li *et al. Journal of Neuroinflammation*   (2023) 20:249

Page 3 of 16

dose–response effect of Slit2 on T cell chemotaxis previously reported in in vitro study [30] and we examined the effects of two additional doses to determine the optimal dose for GMH. The P7 rat pups ($n=30$, 6/group) were randomly divided into five groups: sham, GMH+vehicle, GMH+Slit2 (1 μg/kg), GMH+Slit2 (3 μg/kg), and GMH+Slit2 (10 μg/kg). Short-term neurological assessment was performed during 1–3 days after GMH and brain samples were collected for Western blot analysis on day 5. Additionally, another set of rats were randomly divided into three groups: sham, GMH+Vehicle, and GMH+Slit2 (10 μg/kg), in which Western blotting was performed to validate the delivery efficiency of intranasal administration of Slit2 (10 μg/kg, $n=12$, 4/group) and apoptosis marker cleaved caspase 3 ($n=24$, 6/group); TUNEL staining ($n=18$, 3/group) was used to assess neuron death.

Experiment 4

The role of Robo1 and srGAP1 in recombinant Slit2-mediated protection after GMH was investigated. Rats pups ($n=54$, 6/group) were randomly divided into six groups: sham, GMH+vehicle, GMH+Slit2 (10 μg/kg), GMH+Slit2 (10 μg/kg)+Robo1 (3 μg/kg), GMH+Slit2 (10 μg/kg)+srGAP1 siRNA, and GMH+Slit2 (10 μg/kg)+scrambled siRNA, of which a set of 36 rats were used for long-term neurobehavioral evaluation and another set of 18 from last three groups with shared brain sampled from experiment 2 were used for Western bloting and Cdc42 activity assays. Recombinant Robo1 (3 μg/kg) (R&D Systems, Minneapolis, MN, USA) was co-administered with recombinant Slit2 by intranasal route at 1 h after GMH and daily for 3 consecutive days. srGAP1 siRNA or scrambled siRNA (Life Technologies, Grand Island, NY, USA) was administered via intracerebroventricular (i.c.v.) injection at 24 h before GMH. Brain samples were collected on day 5 for Western blotting and Cdc42 activity assay. Long-term neurological function was evaluated between 21 and 28 days after GMH.

GMH model and treatments

As previously described, we induced grade III or IV GMH by stereotactic infusion of 0.3U bacterial collagenase into the right ganglion bulge of rat pup [31]. In short, the rat pups were anesthetized with 3% isoflurane (mixed air and oxygen) and placed on a stereotactic headframe. All animal operations were performed using aseptic techniques. The anterior horn was found after a small incision in the longitudinal midline of the scalp. With respect to the front corner, a 1-mm burr hole was formed at 1.6 mm on the nozzle side and 1.5 mm on the right side. The No. 27 needle was inserted at the depth of 2.8 mm from the burr hole in a stereotactic manner and

collagenase (1 μl, 0.3 U/μL) was injected (1 μL/min). The needle stayed in place for another 5 min to prevent collagenase from flowing back along the needle path. After the syringe was withdrawn, the burr hole was sealed with bone wax and the incision was closed with suture. The sham animals received the same procedure, except for the infusion of collagenase.

Recombinant Slit2 (6μL; 1, 3, and 10 μg/kg) or vehicle (phosphate-buffered saline, PBS) was administered intranasally at 1 h and daily for 3 consecutive days after GMH induction. Recombinant Robo1, used as a decoy receptor, was co-administered with recombinant Slit2. Slit2 siRNA, srGAP1 siRNA, or scrambled sequence were administered by i.c.v. injection (20μL, 250 pmol/μL, 1 μL/min) 24 h prior to GMH at the following coordinates relative to bregma: 1.0 mm (rostral), 1.0 mm (left lateral), and 1.8 mm (in depth).

Preparation of brain tissues

At 5 days after GMH induction, deeply anesthetized (5% isoflurane) animals were subjected to transcardial perfusion with ice-cold PBS for Western blotting or with ice-cold PBS followed by 10% formalin for immunohistochemical assays. The forebrain was rapidly frozen in liquid nitrogen, preserved at − 80 °C (for Western blotting) or fixed at 10% formalin for 3 days followed by dehydration with sucrose solution (30%) at 4 °C for 3 days (for immunofluorescence). The forebrain sample for immunofluorescence was embedded in the optimal cutting temperature compound and preserved at − 20 °C.

Protein extraction and Western blotting

Forebrain samples were dissolved within RIPA lysis buffer (Santa Cruz Biotechnology, Dallas, TX, USA), and supernatants from the homogenates were collected after centrifugation at 15,000 RPM at 4 °C for 30 min. Protein concentrations were determined using a detergent compatibility assay kit (Bio-Rad, Irvine, CA, USA). Thirty micrograms of protein per sample were loaded into wells of 4–20% gels, run for 30 min at 80 V and then 60 min at 120 V, followed by protein transfer onto 0.45 mm nitrocellulose membranes for 60–120 min (Bio-Rad, Hercules, CA, USA). The membranes were incubated for 2 h in 5% nonfat milk in Tris-buffered saline containing 0.1% Tween 20. The following primary antibodies were incubated overnight at 4 °C: anti-Slit2 (cat: ab7665, 1:1000), anti-myeloperoxidase (MPO) (cat: ab65871, 1:1000), anti-IL-6 (cat: ab9324, 1:1000), anti-TNF-α (cat: ab6671,1:1000), anti-Cleaved Caspase-3(cat: ab2302, 1:500) (all from Abcam, Cambridge, MA, USA), anti-Robo1(cat: sc-25672, 1:200), anti-Macrophage/Monocytes (cat: sc-59103, 1:200), and anti-ICAM1(cat: sc-8439, 1:200) (both from Santa Cruz Biotechnology,

Li *et al. Journal of Neuroinflammation*   (2023) 20:249

Page 4 of 16

Dallas, TX, USA). Anti-β-actin antibodies (cat: sc-69879, 1:1000; Santa Cruz Biotechnology, Dallas, TX, USA) were used as loading control. Membranes with proper secondary antibodies (cat: sc-2357/ sc-525409, 1:4000, Santa Cruz Biotechnology, Dallas, TX, USA) were incubated for 1 h at room temperature. Then enhanced chemiluminescent solution (GE Healthcare and Life Science, Piscataway, NJ, USA) was applied to membranes. Protein exposed to X-ray photographic films were analyzed by ImageJ software (4.0, Media Cybernetics, Silver Spring, MD, USA) for the relative density.

Immunofluorescent staining
Following PBS perfusion and post-fixation of the forebrain samples in formalin, 10-µm-thick coronal sections were cut using a cryostat (Leica Microsystems LM3050S, Wetzlar, Germany). Immunofluorescence staining was performed as previously described [24]. Briefly, the sections were incubated overnight at 4 °C with the following primary antibodies: anti-Slit2 (cat: ab7665, 1:100), anti-neuronal nuclei (NeuN, cat: ab104224, 1:200, neuron marker), anti-glial fibrillary acidic protein (GFAP, cat:ab279290, 1:200, astrocyte marker), anti-myeloperoxidase (MPO, cat: ab65871, 1:200, neutrophil marker) (all from Abcam, Cambridge, MA, USA), anti-Robo1 (cat:sc-25672, 1:100), and anti- differentiation 68 (cat: sc-59103, CD-68, 1:100 macrophages/monocytes marker) (all from Santa Cruz Biotechnology, Dallas, TX, USA). The sections were then incubated with fluorescein isothiocyanate (FITC)-(cat:715-095-151/115-095-003) and Alexa Fluor® 594-conjugated secondary antibodies (cat:115-585-003/711-587-003,1:100; Jackson ImmunoResearch, West Grove, PA, USA) for 1 h at room temperature. TUNEL staining was performed using TUNEL assay kit based on manufacture instruction (cat: C10617; ThermoFisher Scientific, Waltham, MA). All brain slides were visualized using a fluorescence microscope (Olympus BX51, Japan).

For quantitative analysis of immunofluorescent staining, MPO-positive cells within peri-lesion region were counted and averaged from randomly selected three fields of view/brain slice, three brain slices/rat.

Brain water content measurement
Brain edema was evaluated using the wet weight/dry weight method at 24 h after GMH [32]. Briefly, after the animals were killed, the brain was removed immediately, and a coronal tissue slice (4 mm thick) around the injection needle tract was cut. Each section was dissected into three parts: right hemisphere, left hemisphere, and cerebellum. The brain tissue weights were determined

as soon as they were removed and then dried at 100 °C for 24 h to determine the dry weight. Finally, the brain water content (%) in each region was calculated using the following formula: [(wet weight − dry weight)/wet weight] × 100.

Cdc42 activity assay
A pull-down assay was performed using a Cdc42 activity assay kit (cat: STA-402, Cell Biolabs, San Diego, CA, USA) as previously described [33]. Briefly, samples were mixed with p21-activated protein kinase (PAK1)-p21-binding domain (PBD) agarose beads and incubated at 4 °C for 1 h. The beads were resuspended in sample buffer, separated by 10% polyacrylamide gel electrophoresis, and transferred to a nitrocellulose membrane. The membrane was probed with the anti-Cdc42-specific antibody provided in the kit to detect the GTP-bound Cdc42.

Neurobehavioral assessments
Short-term composite Neuroscore
The composite Neuroscore consisted of a sensorimotor value represented by the combined averages from negative geotaxis and righting reflex tests, as previously described [34, 35]. The values are expressed as a percentage of the sham group. The acquisition of developmental milestones was blindly assessed over 3 days. For negative-geotaxis, the time needed for complete rotation (180°) after placing the head down on a slope (20° angle) was recorded [36]. For the righting reflex, the time required for rat pups to completely roll over all four limbs after being placed on their backs was measured [36]. The allotted time was 60 s per trial (two trials/day) for these tests.

Long-term water maze and rotarod tests
Morris water maze and rotarod tests were performed in a blinded manner to evaluate cognitive and sensorimotor deficits in rats between 21 and 28 days after GMH induction as previously described [37].

Simply put, the rats were placed in a circular pool filled with water (110 cm in diameter) and trained to find a visible platform (11 cm in diameter) after these cue trials, the platform was slightly submerged and the rats were allowed to find the location of the platform in 10 trials per day for 4 consecutive days. The platform was removed from the pool at the end (probe trial). An overhead camera with a computerized tracking system (Noldus Ethovision, Noldus, Tacoma, WA, USA) recorded the swimming path and measured the swimming distance and time spent within the probe quadrant.

For Rotarod Test, briefly, rats were placed on a rotarod (Columbus Instruments, Columbus, OH, USA)

Li *et al. Journal of Neuroinflammation*   (2023) 20:249

Page 5 of 16

consisting of a rotating horizontal cylinder (7 cm in diameter). The rats were required to move along the rotating cylinder to avoid falling. Rotarod testing started at either 5 or 10 RPM with an acceleration of 2 RPM every 5 s. A photobeam circuit detected the fall, and the latency of this event was recorded for each animal.

Statistical analysis
Statistical analysis was performed using Sigma Plot 10.0 and Sigma Stat 3.5 (Systat Software, San Jose, CA, USA). Data are presented as mean ± SEM and were evaluated using a one-way ANOVA followed by Tukey's or Student–Newman–Keuls tests. *P* values less than 0.05 were considered statistically significant.

Results
All sham-operated rats survived. One GMH rat died of oxygen deficit. Overall mortality in the total study was 0.64%.

Increased expressions of endogenous Slit2, Robo1 and srGAP1 in brain following GMH
A time-course study was conducted to determine the brain expressions of Slit2, Robo1 and srGAP1 on days 1, 3, 5, and 7 following GMH. Endogenous brain protein expression levels of Slit2 and srGAP1 were increased on day 5 and persisted on day 7 following GMH ($P < 0.05$ sham vs. GMH; Fig. 1A, B, D). Similarly, endogenous brain Robo1 protein expression level was significantly increased and peaked on day 3 after GMH ($P < 0.05$ sham vs. GMH; Fig. 1A, C).

Cell co-localization of endogenous Slit2 and Robo1 in brain following GMH
Double-immunofluorescence staining showed that Slit2 was expressed on neurons and astrocytes (Fig. 2A) on day 5 after GMH. Robo1 was also expressed on both neurons and astrocytes (Fig. 2B). Furthermore, Robo1 colocalized with MPO positive neutrophils and CD68-positive macrophages in the brain tissues (Fig. 2C). Low magnification microphotographs showed relatively even distribution characteristics of Robo1-positive
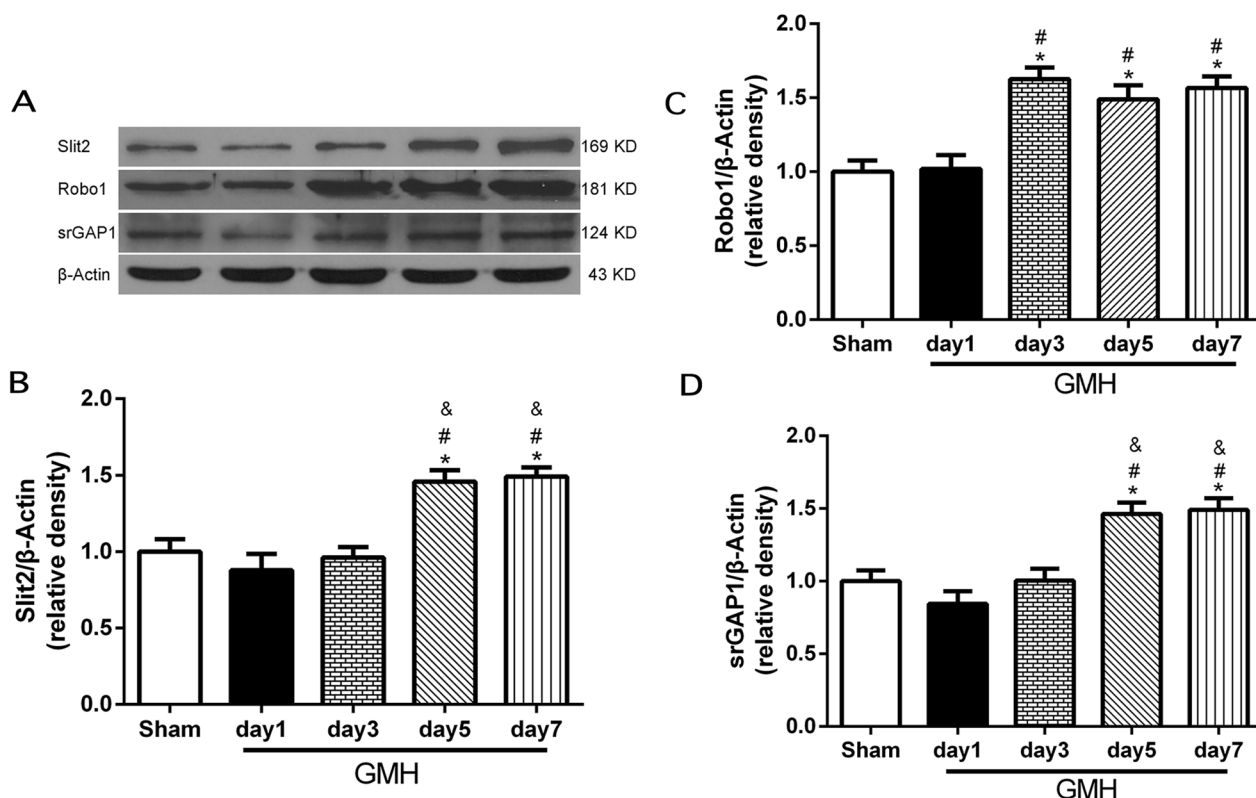

Fig. 1 Expression of endogenous Slit2, Robo1 and srGAP1 in the brain after GMH. Representative Western blotting images (**A**) and quantitative analysis showed that an increased Slit2 expression at day 5 and day 7 after GMH (**B**), an increased Robo1 expression at day 3, day 5 and day 7 after GMH (**C**), and an increased srGAP1 expression at day 5 and day 7 after GMH (**D**). N = 6/group. Mean ± SEM. ANOVA, Tukey. *$P < 0.05$ vs. Sham, #$P < 0.05$ vs. GMH day 1, &$P < 0.05$ vs. GMH day 3

Li *et al. Journal of Neuroinflammation*   (2023) 20:249
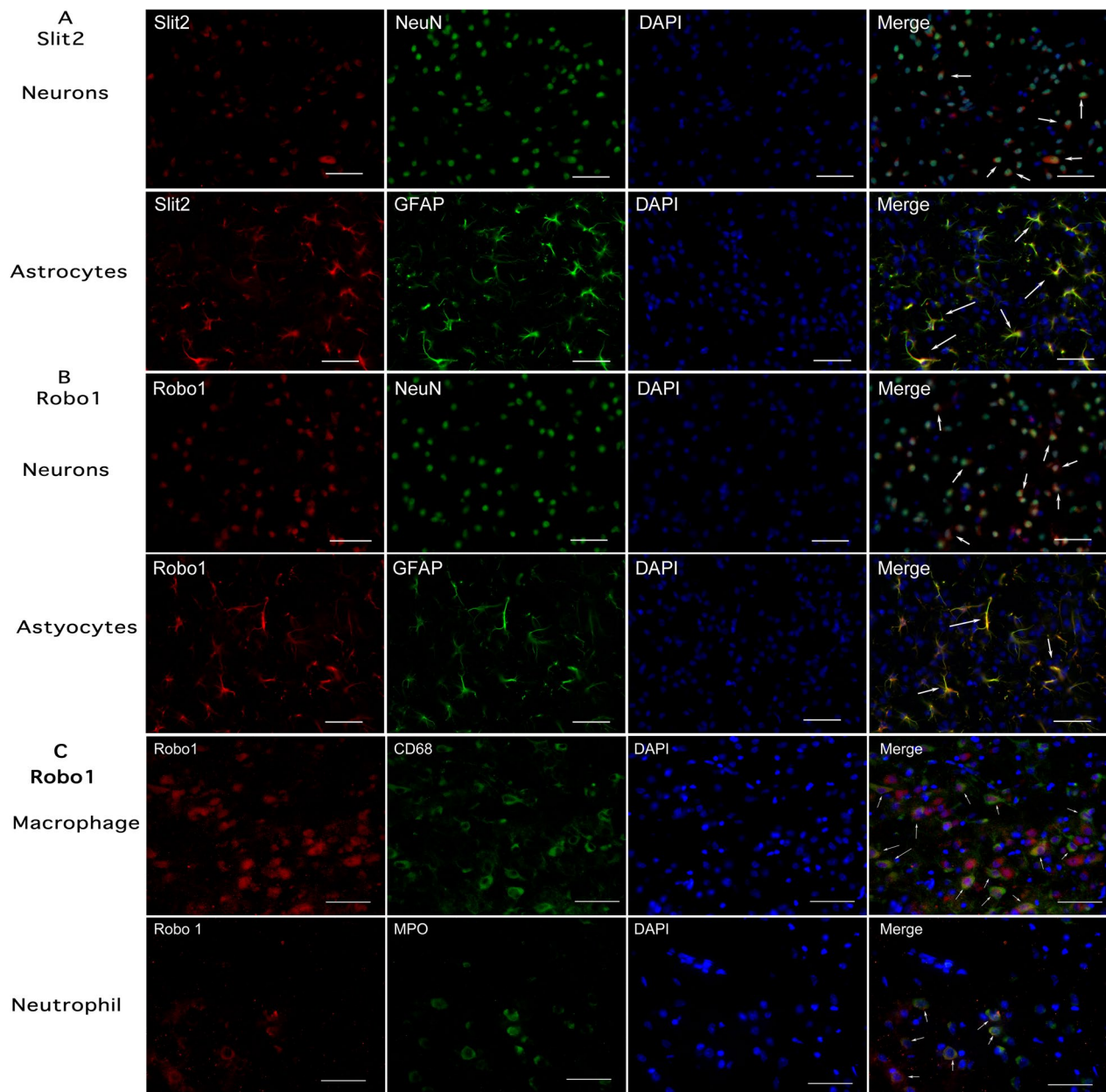
Page 6 of 16

Fig. 2 Cellular locations of Slit2 and Robo1 in brain at 5 days after GMH. Representative microphotograph of immunofluorescence staining showed a co-localization of Slit2 (**A**) and Robo1 (**B**) with neuron (NeuN) or astrocyte (GFAP), respectively. Scale bar = 100 µm. Robo1 (**C**) was colocalized with infiltrating CD68-positive macrophages or MPO positive neutrophil, respectively. Scale bar = 200 µm. Arrows indicate merged cells

staining at peri-lesion and areas remote to lesion (Additional file 1: Fig. S1).

Knockdown of endogenous brain Slit2 worsened brain edema and short-term neurobehavioral deficits following GMH

Slit2 knockdown by Slit2 siRNA effectively suppressed the brain expression of Slit2 ($P < 0.05$ GMH + Slit2 siRNA vs. GMH + scramble siRNA, GMH; Fig. 3A). Brain water content of ipsilateral (right) hemisphere was significantly increased at 24 h after GMH ($P < 0.05$ sham vs. GMH; Fig. 3B). GMH rats that received Slit2 siRNA had significantly higher brain water content ($P < 0.05$ GMH + Slit2 siRNA vs. GMH + scramble siRNA, GMH + Vehicle; Fig. 3B). The negative-geotaxis test showed worse neurological function in the GMH + Slit2 siRNA group than
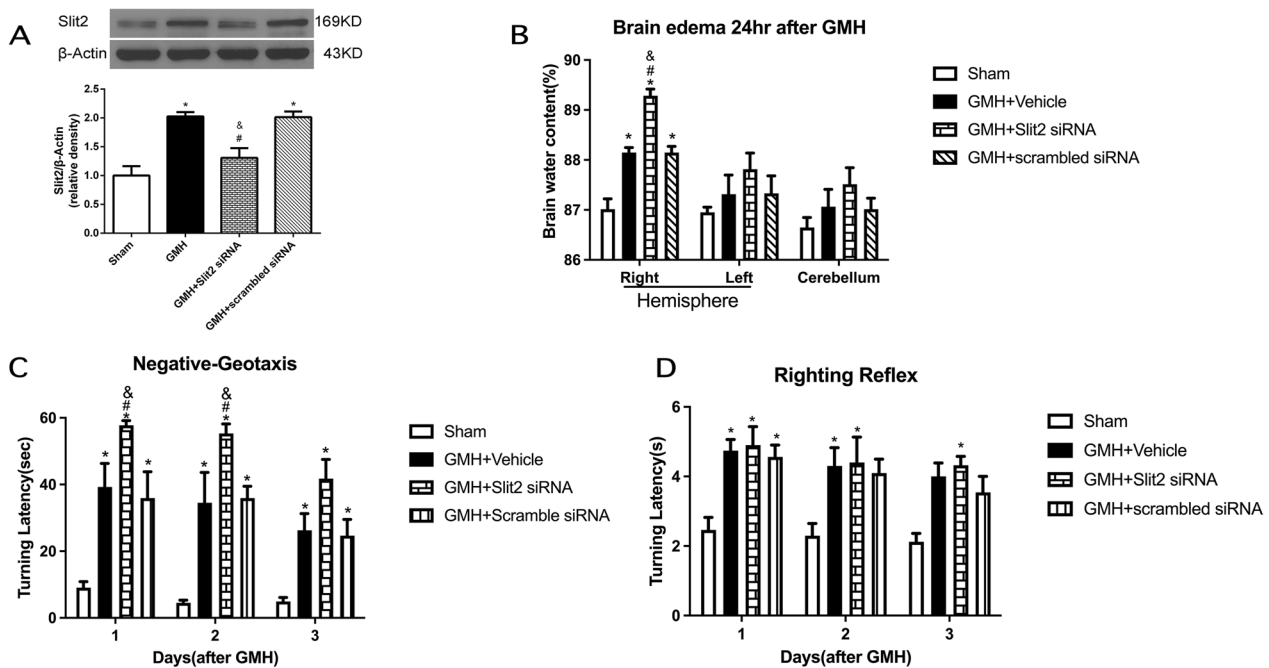
Li *et al. Journal of Neuroinflammation*   (2023) 20:249

Page 7 of 16

Fig. 3 Effects of endogenous brain Slit2 knockdown in GMH. **A** Representative Western blotting image and quantitative analysis showed that Slit2 siRNA significantly reduced the brain Slit2 expression. Endogenous brain Slit2 knockdown worsened brain edema at 24 h after GMH (**B**) and aggravated neurobehavioral performance in the negative-geotaxis test (**C**) at 1 day and 2 days after GMH. **D** There was not significant different among all GMH groups in righting-reflex test during the 3 days after GMH. $N = 6$/group. Mean ± SEM. ANOVA, Tukey. *$P < 0.05$ vs. Sham, #$P < 0.05$ vs. GMH + Vehicle, &$P < 0.05$ vs. GMH + scrambled siRNA

that in the GMH + scrambled siRNA group at 1 and 2 day after GMH ($P < 0.05$; Fig. 3C). However, there were no significant differences among the groups in the righting reflex test during 3 days after GMH (Fig. 3D).

Recombinant Slit2 administration improved short-term neurological deficits following GMH

Short-term neurological function evaluated by the negative-geotaxis (Fig. 4A) and righting reflex (Fig. 4B) tests worsened on days 1, 2 and 3 after GMH ($P < 0.05$ sham vs. GMH + Vehicle). Although all doses of rSlit2 improved

negative-geotaxis and righting reflex performances from day 1 to 3 after GMH, only rSlit2 10 µg/kg showed a significant result at day 1 and 2 ($P < 0.05$ GMH + Vehicle vs. GMH + Slit2). In addition, the delivery efficiency of intranasal administration of rSlit2 (10 µg/kg) was validated. After intranasal administration of rSlit2, Slit2 expression was significantly higher in the rSlit2 treated GMH group than that in the vehicle treated GMH group on day 5 ($P < 0.05$; Fig. 4C), indicating that intranasally administered rSlit2 (10 µg/kg) was successfully delivered into the brain.
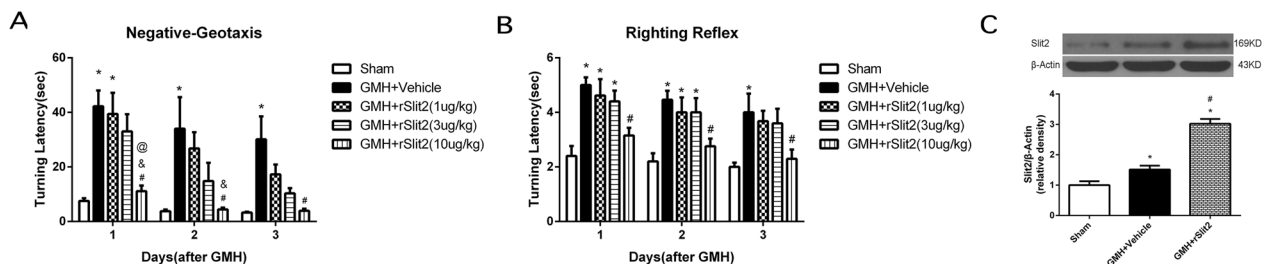

Fig. 4 Effects of recombinant Slit2 on neurobehavior after GMH. Recombinant Slit2 (10 µg/kg) improved the performance in the negative-geotaxis (**A**) and righting-reflex (**B**) at 1, 2 and 3 days after GMH. N = 6/group. *$P < 0.05$ compared to Sham, #$P < 0.05$ compared to GMH + Vehicle, rSlit2 (1 µg/kg), rSlit2 (3 µg/kg). **C** Brain Slit2 expression was increased in the rSlit2 treatment group, indicating that rSlit2 (10 µg/kg) was successfully delivered into the brain by intranasal administration. $N = 4$/group. Mean ± SEM. ANOVA, Tukey. *$P < 0.05$ vs. Sham, #$P < 0.05$ vs. GMH + Vehicle
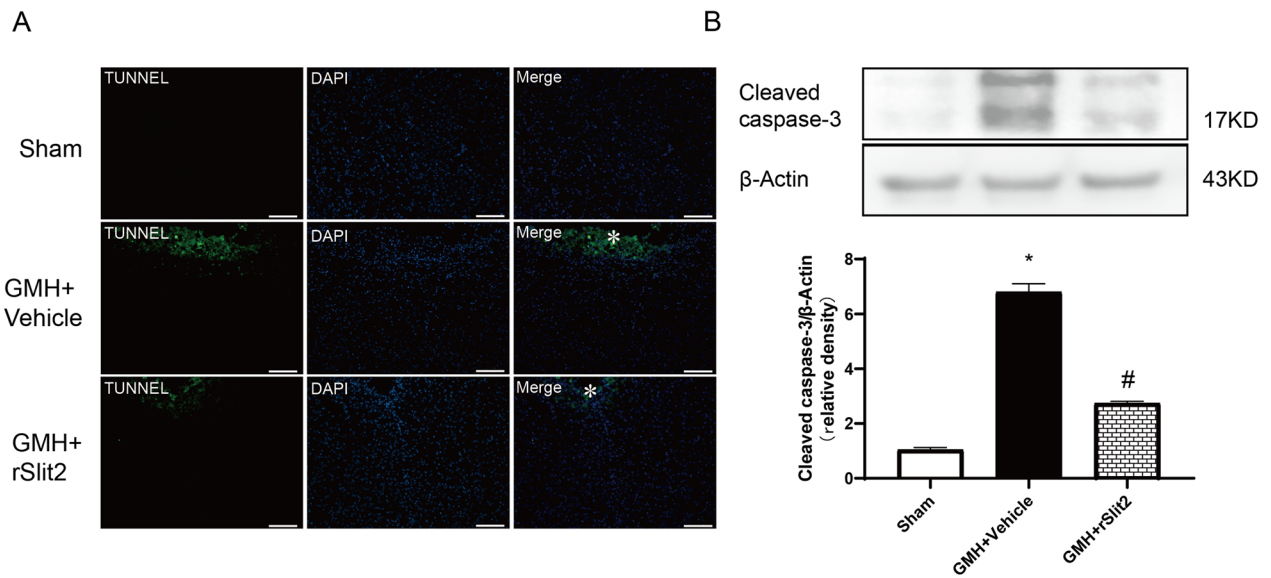
Li *et al. Journal of Neuroinflammation*   (2023) 20:249

Page 8 of 16

Fig. 5 Effects of recombinant Slit2 on neuronal death in brain at 5 days after GMH. TUNEL staining showed the degree of DNA breakage (**A**) was aggravated after GMH, which were reduced by rSlit2. "*" symbol indicates the lesion location on the representative microphotograph of brain slice. Scale bar = 100 μm. Western blotting image and quantitative analysis showed that brain cleaved caspase-3 (**B**) expressions increased after GMH, which were reduced by rSlit2. N = 6/group. Mean ± SEM. ANOVA, Tukey. *$P < 0.05$ vs. Sham, #$P < 0.05$ vs. GMH + Vehicle

Recombinant Slit2 reduced neuronal death following GMH

There were TUNEL-positive staining at 5 days after GMH, reduced in rSlit2 10 μg/kg-treated GMH rats (Fig. 5A). Similarly, in the brain tissue of GMH rats, there was a significant increase in cleaved caspase-3 protein level ($P < 0.05$ sham vs. GMH; Fig. 5B), while rSlit2 decreased it ($P < 0.05$ GMH + Vehicle vs. GMH+rSlit2; Fig. 5B). rSlit2 treatment effects on TUNEL-positive staining and cleaved caspase-3 protein level in the brain tissues were also observed at 1 day after GMH (Additional file 1: Fig. S2).

Recombinant Slit2 reduced brain expressions of proinflammatory cytokines/chemokines and neutrophil infiltrations following GMH

The expressions of proinflammatory cytokines/chemokines TNF-α, IL-6, and ICAM-1 in the brain was quantified using Western blotting at 5 days after GMH. Protein expression levels were significantly higher after GMH ($P < 0.05$ sham vs. GMH + Vehicle; Fig. 6A–C). Recombinant Slit2 10 μg/kg significantly reduced the upregulations of brain TNF-α, IL-6, and ICAM-1 after GMH ($P < 0.05$ GMH + Vehicle vs. GMH + rSlit2).
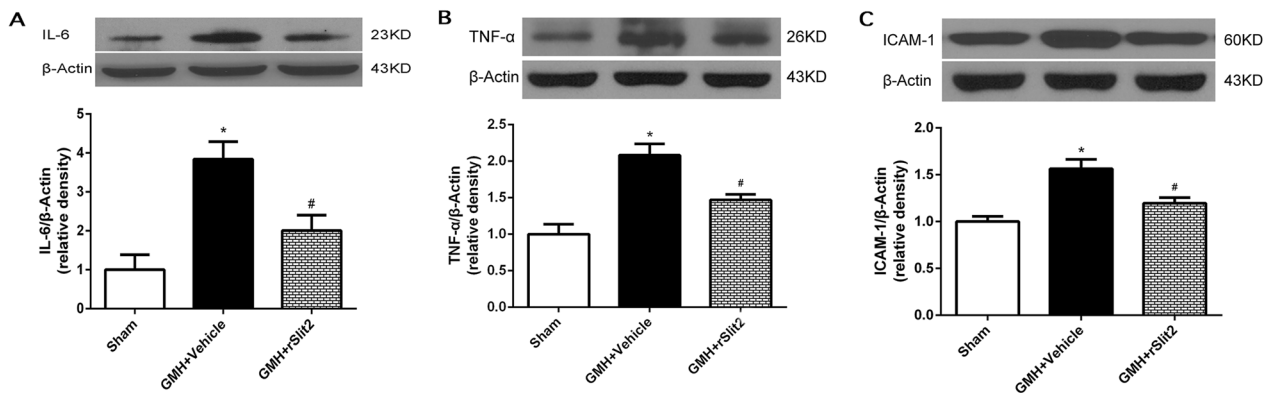

Fig. 6 Effects of recombinant Slit2 on proinflammatory cytokines in brain at 5 days after GMH. Western blotting image and quantitative analysis showed an increase in brain IL-6 (**A**), TNF-α (**B**) and ICAM-1 (**C**) expressions after GMH, which were reduced by recombinant Slit2 treatment. N = 6/group. Mean ± SEM. ANOVA, Tukey. *$P < 0.05$ vs. Sham, #$P < 0.05$ vs. GMH + Vehicle

Li *et al. Journal of Neuroinflammation*   (2023) 20:249

Page 9 of 16

Immunofluorescence staining showed greater MPO-positive cells in brains of GMH rats than shams, but there were fewer cells positively stained for MPO in the brain of rSlit2 (10 μg/kg)-treated GMH animals than that of the vehicle-treated GMH animals at 1 day (Additional file 1: Fig. S3A) and at 5 day (Fig. 7A and Additional file 1: Fig. S3B) after GMH.

Beneficial effects of recombinant Slit2 following GMH were reversed by recombinant Robo1 co-administration or srGAP1 siRNA

We investigated the role of Robo1–srGAP1 pathway in rSlit2-mediated anti-inflammation after GMH. The expression of neutrophil marker MPO (Fig. 7A, B), and macrophage marker CD68 (Fig. 7C) were significantly increased after GMH ($P < 0.05$ sham vs. GMH + Vehicle; Fig. 7). rSlit2 (10 μg/kg) significantly reduced the expression of both markers ($P < 0.05$ GMH + Vehicle vs. GMH + rSlit2; Fig. 7). Either recombinant Robo1 co-administration or srGAP1 siRNA abolished the effects of
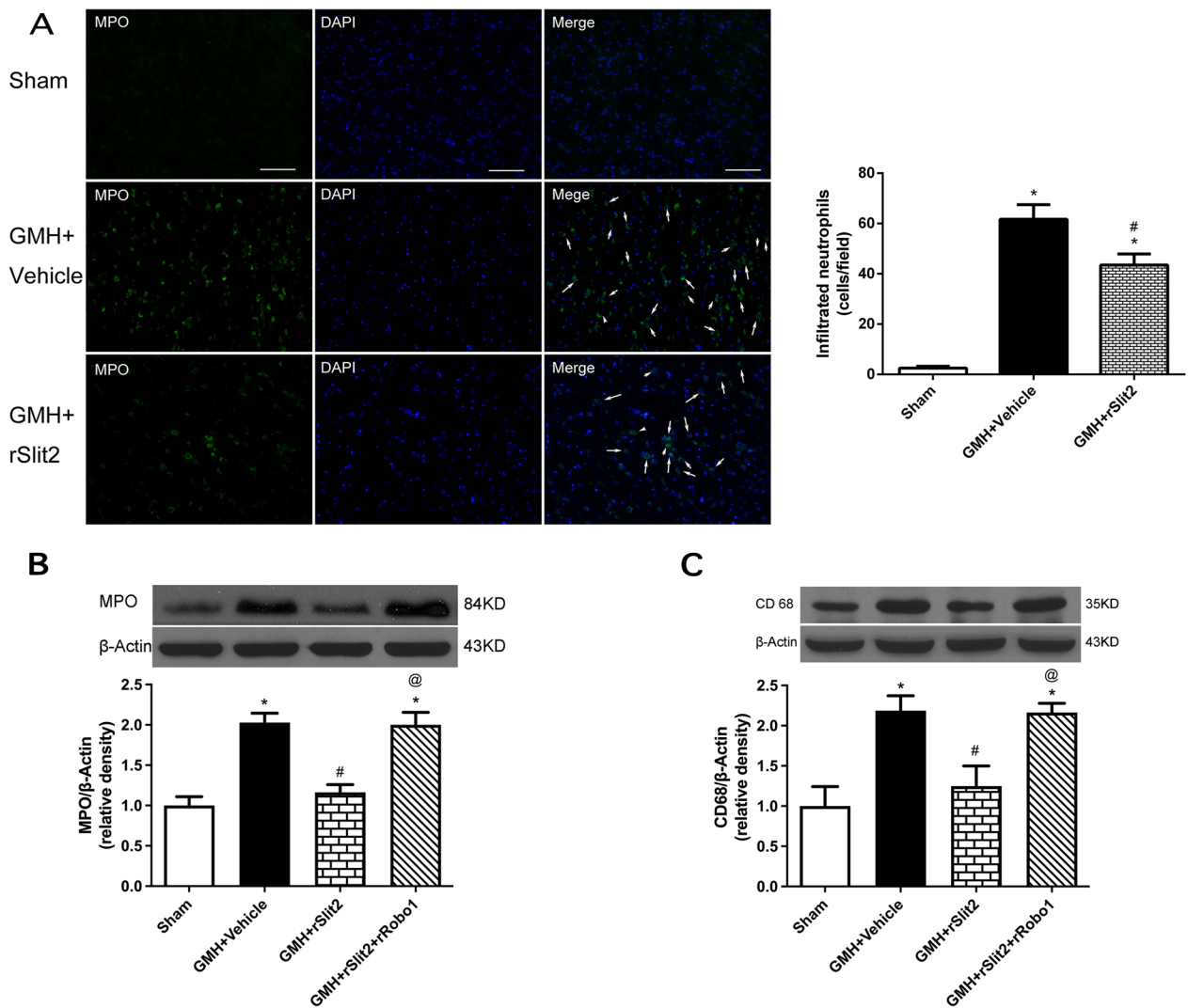

Fig. 7 Effects of recombinant Slit2 on brain peripheral immune cells infiltration at 5 days after GMH. **A** Representative microphotograph and quantitative analysis of immunofluorescence staining showed that fewer MPO positive neutrophils were visualized in the brain tissue of GMH+rSlit2 group compared to GMH+Vehicle group. Scale bar = 100 μm; Western blotting analysis showed that recombinant Slit2 down-regulated brain neutrophil marker MPO (**B**) and macrophage marker CD68 (**C**) after GMH and such effects were reversed by rRobo1 co-administration. $N = 6$/group. Mean ± SEM. ANOVA, Tukey. *$P < 0.05$ vs. Sham, #$P < 0.05$ vs. GMH+Vehicle, @$P < 0.05$ vs, GMH+rSlit2

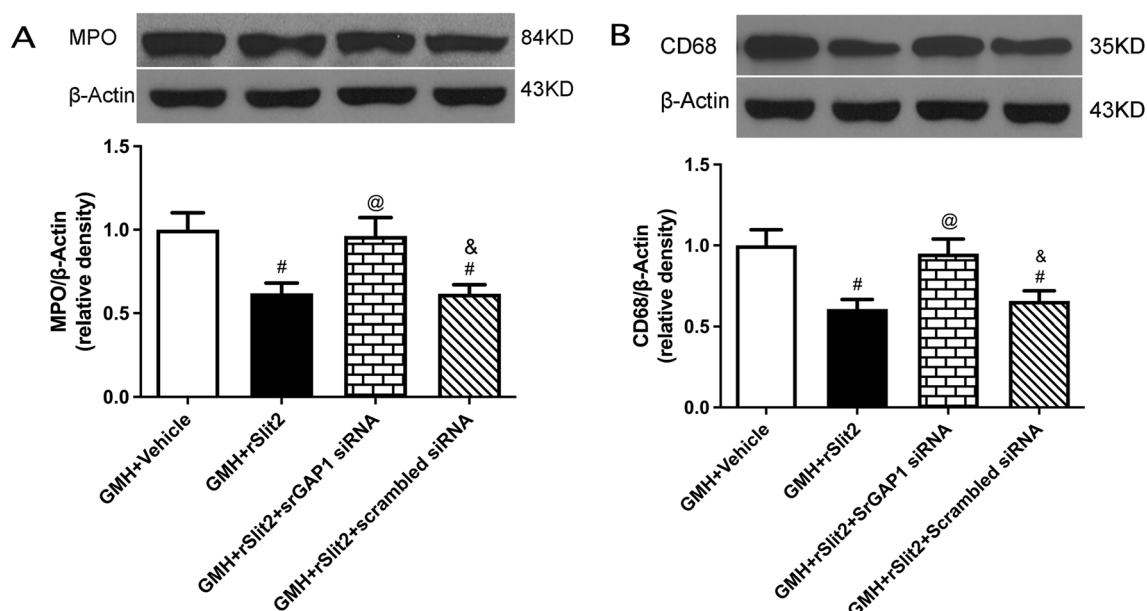Li *et al. Journal of Neuroinflammation*   (2023) 20:249

Page 10 of 16

Fig. 8 Effects of srGAP siRNA on recombinant Slit2-mediated downregulation of peripheral immune cells infiltration into brain. Western blotting analysis showed that the downregulation of brain MPO (**A**) and CD68 (**B**) expressions by recombinant Slit2 were reversed by srGAP1 siRNA in GMH rats. N=6/group. Mean±SEM. ANOVA, Tukey. #$P < 0.05$ vs. GMH+Vehicle, @$P < 0.05$ vs. GMH+rSlit2. &$P < 0.05$ vs. GMH+rSlit2+srGAP1 siRNA

recombinant Slit2 with higher expressions of MPO and CD68 ($P < 0.05$ GMH + Slit2 vs. GMH + Robo1+rSlit2, Fig. 7; $P < 0.05$ GMH + rSlit2 vs. GMH + srGAP1 siRNA+rSlit2, Fig. 8). The lower magnification microphotograph showed that neutrophils are concentrated in peri-lesion area (Figure S3). Similar to Day 5, MPO-positive cells were evident in the peri-lesion area of GMH rats on day 1, which was reduced by rSlit2 treatment (Additional file 1: Fig. S3).

Co-administration of recombinant Robo1 with recombinant Slit2 reversed the rSlit2 effects on both brain expressions of Robo1 and srGAP1 after GMH ($P < 0.05$ GMH+rSlit2 vs. GMH+rSlit2+rRobo1; Fig. 9A). The administration of srGAP1 siRNA reversed rSlit2 effect on brain srGAP1expression, but had no effect on the brain protein level of Robo1 ($P < 0.05$ GMH+rSlit2 vs. GMH+rSlit2+srGAP1 siRNA; Fig. 9B).

Long-term neurobehavioral function was evaluated using the Morris water maze and rotarod tests on days 21–28 after GMH. Animals of GMH+Vehicle, GMH+rSlit2+Robo1, and GMH+rSlit2+srGAP1 siRNA groups took a longer period of time to find the platform than sham animals in the Morris water maze trials ($P < 0.05$; Fig. 10A). Furthermore, animals in the GMH+Vehicle group spent less time in the target quadrant during the probe trials than the animals in the sham group ($P < 0.05$ sham vs. GMH+Vehicle; Fig. 10B). Animals received rSlit2 treatment spent more time in the target quadrant during the probe trials than vehicle-treated

animals ($P < 0.05$). However, there were no significant differences in other groups. Similarly, animals in groups of GMH+Vehicle, GMH+rSlit2+rRobo1, and GMH+rSlit2+srGAP1 siRNA fell off the rotating cylinder earlier than the sham animals at a starting speed of 5 RPM ($P < 0.05$; Fig. 10C). Animals receiving recombinant Slit2 treatment performed better on the rotarod test than the animals in the vehicle group ($P < 0.05$).

The inhibition effects of recombinant Slit2 on Cdc42 activity following GMH were reversed by recombinant Robo1 co-administration or srGAP1 siRNA

Brain Cdc42 activity was significantly increased at 5 days after GMH ($P < 0.05$ sham vs. GMH + Vehicle+ GMH; Fig. 11A), which was reduced in rSlit2 10 µg/kg-treated GMH rats ($P < 0.05$ GMH+ Vehicle vs. GMH + rSlit2). Recombinant Robo1 (3 µg/kg) partially reversed the reduction in Cdc42 activity induced by rSlit2 ($P < 0.05$ GMH+Robo1+rSlit2 vs. GMH+rSlit2 10 µg/kg; Fig. 11A). srGAP1 siRNA also reversed the reduction in brain Cdc42 activity induced by rSlit2 ($P < 0.05$ GMH + srGAP1 siRNA vs. GMH + rSlit2, GMH + rSlit2 +scramble siRNA; Fig. 11B).

Discussion

In this study, we investigated the therapeutic potential of recombinant Slit2 protein in suppressing the neuroinflammatory response following GMH in rats. We observed that the brain expression of endogenous Slit2
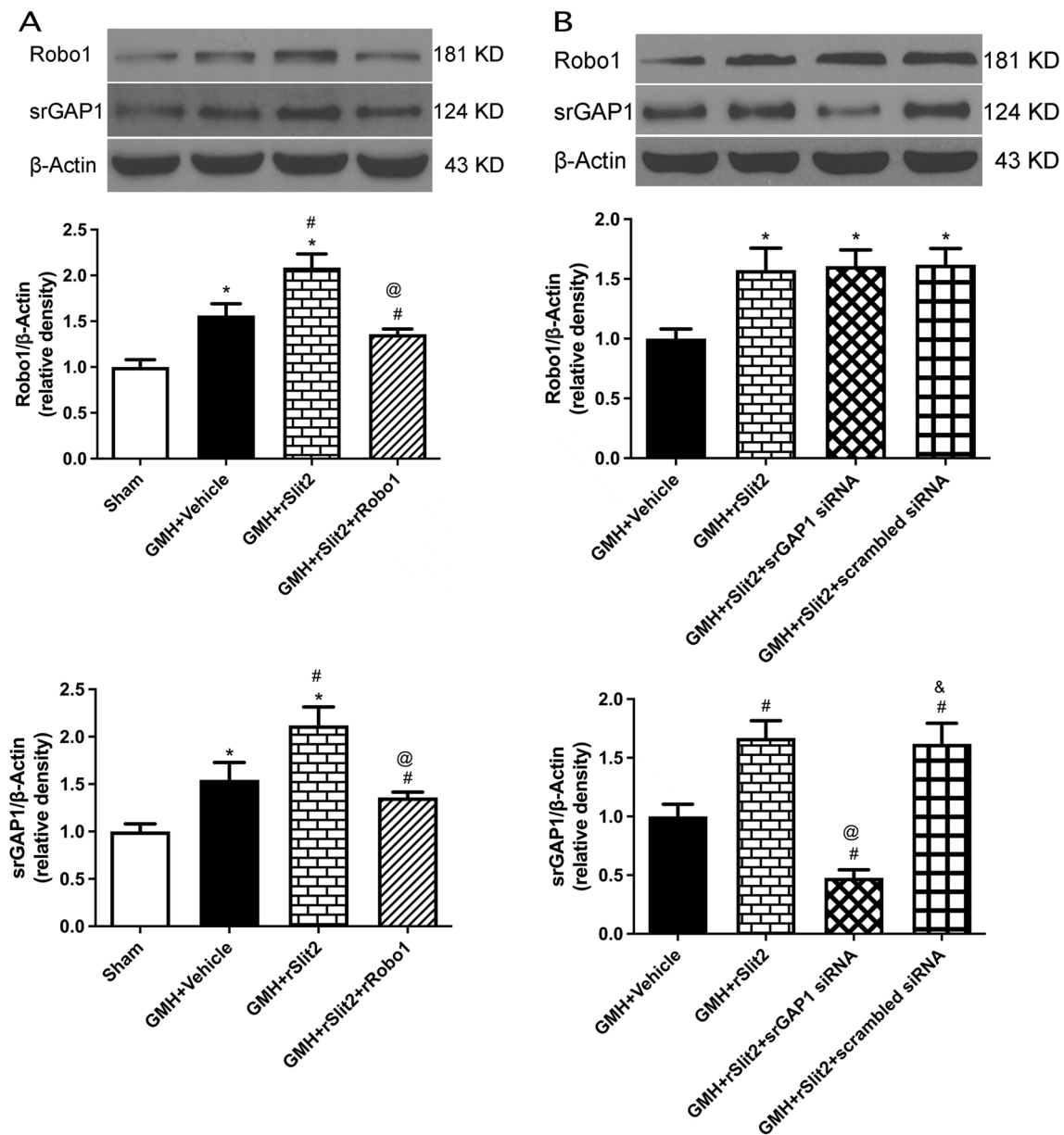
Li *et al. Journal of Neuroinflammation*   (2023) 20:249

Page 11 of 16

Fig. 9 Western blotting analysis of brain Robo1 and srGAP1 expressions at 5 days after GMH. **A** Brain expressions of Robo1 and srGAP1 were significantly increased after GMH compared to Sham, which were further elevated in GMH + rSlit2 group. Recombinant Robo1 co-administration with rSlit2 reversed the upregulation effects of rSlit2 of on Robo1 and srGAP1. **B** Brain srGAP1 expression was increased in GMH + rSlit2 and GMH + Slit2 + scrambled siRNA groups compared to GMH. The administration of srGAP1 siRNA decreased the expression of srGAP1, but not Robo1 in brain after GMH. $N = 6$/group. Mean ± SEM. ANOVA, Tukey. *$P < 0.05$ vs. Sham, #$P < 0.05$ vs. GMH + Vehicle, @$P < 0.05$ vs. GMH + rSlit2, &$P < 0.05$ vs. GMH + rSlit2 + srGAP1 siRNA

was significantly increased after GMH. The knockdown of endogenous brain Slit2 exacerbated GMH-induced brain edema and short-term neurological deficits. Recombinant Slit2 treatment after GMH attenuated neuronal death, neuroinflammation and neurological deficits, but inhibited Cdc42 activity and reduced the cerebral infiltration of peripheral immune cells after GMH.

The beneficial effects of rSlit2 treatment were reversed by co-administration with the decoy receptor rRobo1 or the siRNA knockdown of downstream effector srGAP1 in the brain. According to these results, brain Slit2 signaling might provide an endogenous protective effect after GMH, and rSlit2 may serve as promising therapeutics to attenuate neuroinflammation after GMH.
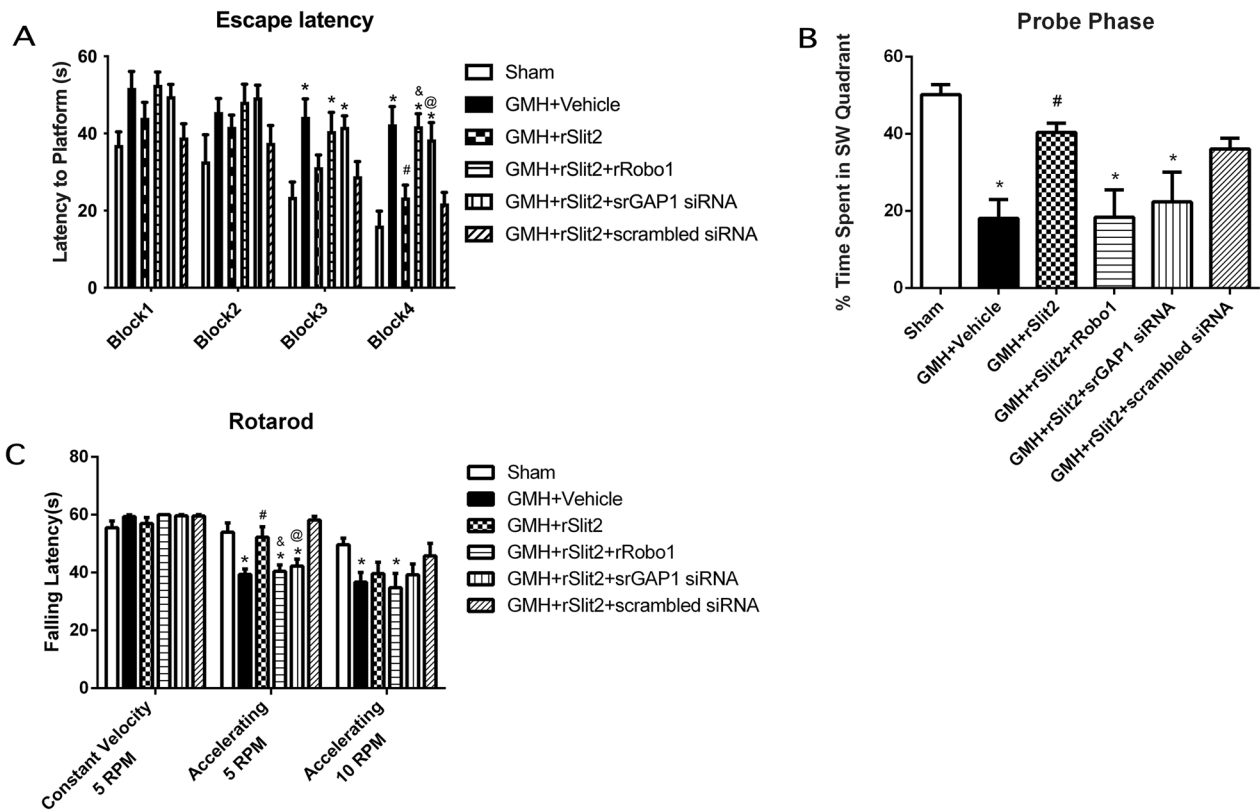
Fig. 10 Effects of recombinant Slit2 on long-term neurobehaviors after GMH. Recombinant Slit2 improved the performances on Water Maze test (**A**, **B**) and Rotarod test (**C**) in GMH rats, which were reversed either by co-administration of rRobo1 or srGAP1 siRNA. $N=6$/group. Mean ± SEM. ANOVA, Tukey. $*P < 0.05$ vs. Sham, $^{\#}P < 0.05$ vs. GMH+Vehicle, $^{\&}P < 0.05$ vs. GMH+rSlit2, $^{@}P < 0.05$ vs. GMH+rSlit2+scrambled siRNA
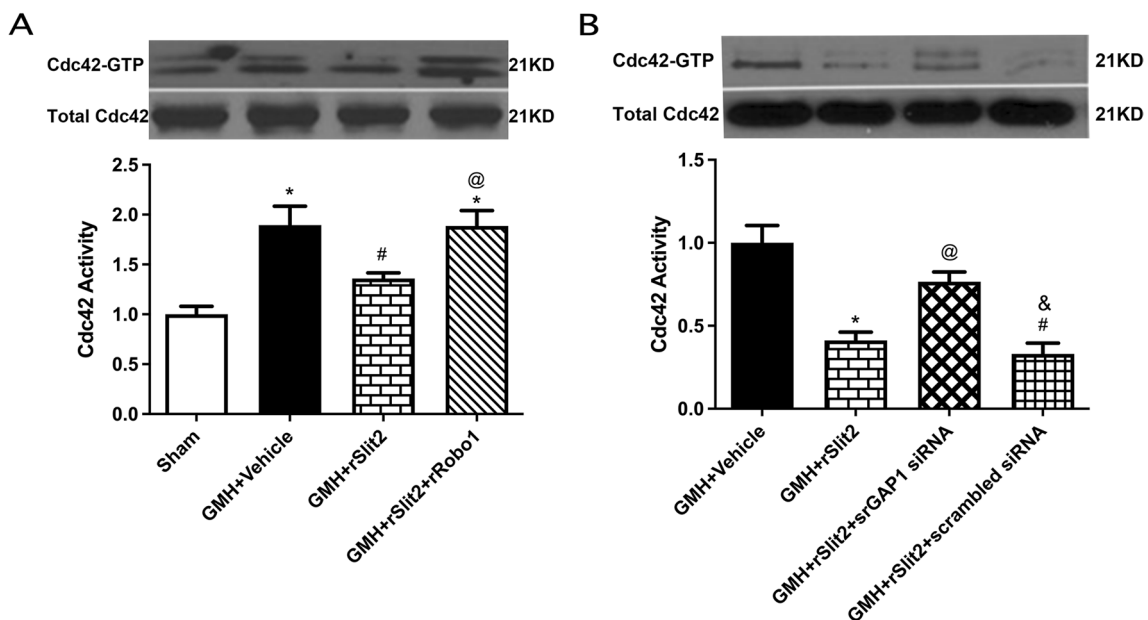

Fig. 11 Brain Cdc42 activity assessment at 5 days after GMH. **A** There was an elevation of Cdc42 activity in brain after GMH, which reduced by recombinant Slit2 treatment. Recombinant Robo1 co-administration blocked the inhibition effect of recombinant Slit2 on brain Cdc42 activity. **B** srGAP1 siRNA, but not scrambled siRNA, blocked the inhibition effect of recombinant Slit2 on brain Cdc42 activity. $N=6$/group. Mean ± SEM. ANOVA, Tukey. $*P < 0.05$ vs. Sham, $^{\#}P < 0.05$ vs. GMH+Vehicle, $^{@}P < 0.05$ vs. GMH+rSlit2, $^{\&}P < 0.05$ vs. GMH+rSlit2+srGAP1 siRNA

Slit2 is a chemorepulsive element that facilitates axonal guidance and neuronal migration in the central nervous system (CNS) during development [38, 39]. The inflammatory responses in several systemic conditions, such as renal, peritoneal, and lung inflammation, have been demonstrated to be inhibited by Slit2 in many preclinical studies [40–42]. However, its efficacy in neuroinflammation in the context of GMH is still unclear. This study showed that endogenous brain Slit2 was increased from day 5 and persisted at day 7 after GMH. This protein localized on neurons and astrocytes in GMH rats. This finding matched earlier research that Slit2 was found to express on neurons and astrocytes [43]. Robo1 is a protein with a single transmembrane domain [44] that serves as a Slit receptor for axon guidance [27] and neuronal migration [19]. Robo1 is also expressed on the leukocyte that mediate the anti-migratory effects of Slit2 [45]. Our results also showed that Robo1 expression was positively correlated with Slit2 expression following GMH. Previous studies indicated the expression of Robo1 on neutrophils [41], lymphocytes [46], and mononuclear macrophages [30]. Consistently, we found that Robo1 was colocalized with infiltrating MPO-positive neutrophils and CD68-positive marcrophages in brains of GMH rats.

Slit was shown to be an endogenous inhibitory factor for leukocytes chemotaxis recently [41]. To clarify the role of endogenous Slit2 after GMH, Slit2 siRNA was used to knockdown the endogenous Slit2 in brain in prior to GMH induction. Endogenous Slit2 knockdown worsened GMH-induced brain edema of the ipsilateral hemisphere and sensorimotor dysfunction in the negative-geotaxis test. The endogenous brain Slit2 seems to be elevated as a potential compensatory mechanism, although the protective effects were not sufficient to counteract brain injury after GMH. Firstly, Slit2 and its receptors including Robo1 and Robo4 are labeled to regulate the mobility and permeability of endothelial cells and other cell types. The brain secretory protein Slit2 can be secreted into the CSF and eventually into the bloodstream. It could directly bind to Robo1 receptors in peripheral immune cells, suppressing their migration to the brain parenchyma [26]. In addition, previous studies have shown that Slit2 can exert anti-inflammatory effects mediated by the dominant endothelial-specific receptor Robo4 [47]. Secondly, immune cells and proinflammatory factors can enter the brain parenchyma without any pathogen [48]. During viral infections or when certain autoimmune disorders develop in the CNS, activated T cells can cross the blood–brain barrier (BBB) and initiate both protective and unwanted inflammatory responses. When

the BBB is damaged, many T cells and other inflammatory cells enter the CNS by encountering perivascular macrophages [48, 49]. Endogenous Slit2 may then be increased to compensate for endothelial barrier breakdown after GMH. By binding to the endothelial-specific receptor Robo4, Slit2 was proven to reduce endothelial barrier permeability [50, 51]. Thus, endogenous Slit2 knockdown worsened the outcomes in GMH rats.

The treatment effects of exogenous recombinant Slit2 were further evaluated after GMH. Three doses of recombinant Slit2 were examined by comparing the outcomes on day 1, day 2, and day 3 after GMH [44]. Recombinant Slit2 at dose of 10 μg/kg improved the overall performance in the negative-geotaxis and righting reflex tests on both days 1 and 2 after GMH. In response to injury, leukocytes accumulate in the CNS [52, 53]. The activated microglia synthesize cytokines and inflammatory mediators that induce endothelial cells to upregulate ICAM-1 [54] and promote peripheral leukocyte adhesion to the brain and potentiates neuroinflammation [55]. Slit2 has been reported to inhibit leukocyte migration induced by chemokines [56, 57]. Our results demonstrated that recombinant Slit2 treatment reduced brain proinflammatory cytokines including TNF-α and IL-6, and ICAM-1, and the expressions of peripheral immune cell markers in brain tissues, such as MPO and CD68, in brain after GMH. Previous study showed recombinant Slit2 reduced neuronal death after experimental neonatal hypoxic-ischemic encephalopathy (HIE) [25]. Consistently, GMH induced neuron death and an increase in brain apoptotic marker at 1 and 5 days after GMH, which were attenuated by recombinant Slit2 treatment. Collectively, our finding suggests rSlit2 improved neurological outcomes by suppressing neuroinflammation and reducing neuronal apoptosis.

To better elucidate the anti-neuroinflammation mechanism of recombinant Slit2, the role of its single transmembrane domain receptor Robo1 [58] was investigated. A previous study showed that recombinant Robo1 acts as a decoy receptor by binding to recombinant Slit2, which resulted in less Slit2 available to bind to the Robo1 receptors on immune cells, thereby reducing its anti-migratory function [24]. In the present study, co-administering recombinant Robo1 with recombinant Slit2 as a decoy receptor neutralized the effects of recombinant Slit2 with increasing peripheral immune cells infiltration into the brain. This suggests that Slit2 regulates peripheral immune cell migration to the brain in a Robo1-dependent manner. Moreover, the downstream effector srGAP1 mediates the inhibitory

Li *et al. Journal of Neuroinflammation*   (2023) 20:249

Page 14 of 16

effects of the Slit2-Robo1 interaction on migration [26]. Slit2 enhances the interaction of the SH3 domain in srGAP1 with the CC3 motif in Robo1, and this localization may induce inactivation of a small GTPase protein Cdc42, a member of the Rho-GTPase family, by converting the active GTP-bound form of Cdc42 to the inactive GDP-bound form of Cdc42 [59]. Cdc42 has been reported to function as a key mediator of cell migration [33]. The interaction between srGAP1 and the GTP-bound activated form of Cdc42 abolishes the directional mobility of the cell toward chemoattractant [17]. Consistently, our data revealed that Cdc42 activity was markedly inhibited by recombinant Slit2. When recombinant Robo1 was co-administered or srGAP1 was knocked down by siRNA, the effects of recombinant Slit2 on the inhibition of Cdc42 activity and peripheral immune cells migration/cerebral infiltration was reversed after GMH. This suggests that recombinant Slit2 may exert its anti-chemotactic and neuroprotective effects by activating the Robo1/ srGAP1 pathway to inhibit Cdc42 activity, which subsequently reduces peripheral immune cells infiltration into the brain after GMH. The activation Slit2/ Robo1/ srGAP1 signaling pathway was also shown to be the anti-apoptosis mechanism in the setting of HIE [25]. Therefore, we could not exclude such anti-neuronal apoptotic mechanism underlying the treatment effects of recombinant Slit2 after GMH, which needs future investigation.

In conclusion, our data showed that the endogenous brain chemorepulsive factor Slit2 was increased and served as a compensatory protective mechanism after GMH in rats. The recombinant Slit2 treatment reduced neuronal death and neuroinflammation. Specifically, the anti-neuroinflammation effect of recombinant Slit2 on suppressing Cdc42-mediated peripheral immune cell infiltration into brain was at least in part via the Robo1/ srGAP1 pathway. These results imply that recombinant Slit2 may have potentials as a therapeutic option for neonatal brain injuries.

Supplementary Information

The online version contains supplementary material available at https://doi.org/10.1186/s12974-023-02935-2.

Additional file 1: Figure S1. Cellular locations of Slit2 and Robo1 in brain at 5 days after GMH. Representative microphotograph of immunofluorescence staining showed a co-localization of Slit2 (**A**) or Robo1 (**B**) with neuron (NeuN) and astrocyte (GFAP) across the brain section,

---

respectively. Co-localization of Robo1 (**B**) with CD68-positive macrophage or MPO positive neutrophil was presented at the peri-lesion brain area. "*" symbol indicates the location of lesion Scale bar=100 μm. **Figure S2.** Effects of recombinant Slit2 on neuronal death in brain at 1 days after GMH. TUNEL staining showed the aggravated degree of DNA breakage (**A**) after GMH, which were reduced by rSlit2 treatment. "*" symbol indicates the location of lesion. Scale bar=100μm. Western blotting image and quantitative analysis showed that brain cleaved caspase-3 (**B**) expressions increased after GMH, which were reduced by rSlit2 treatment. N=6/group. Mean±SEM. ANOVA, Tukey. *$P<0.05$ vs. Sham, #$P<0.05$ vs. GMH+Vehicle. **Figure S3.** Effects of recombinant Slit2 on peripheral immune cells infiltration into brain at 1 and 5 days after GMH. MPO immunofluorescence staining showed that MPO positive neutrophils were concentrated in the peri-lesion area at day 1(**A**) and day 5(B) after GMH, and the number of MPO positive neutrophils were reduced by rSlit2 treatment. The lesion was located in the upper or/and left. Scale bar=100μm.

Availability of data and materials
The original datasets generated and/or analyzed during the current study are available from the corresponding author on reasonable request.

Declarations

Ethics approval and consent to patriciate
Not applicable.

Consent for publication
Not applicable.

Competing interests
The authors declare that they have no competing interests.

Author details
[1]Department of Pediatrics, Army Medical Center, Army Medical University, 10 Changjiang Access Rd, Yuzhong District, Chongqing 400042, China. [2]Women and Children's Hospital of Chongqing Medical University, 120 Longshan Access Rd, Yubei District, Chongqing 400010, China. [3]Department of Physiology and Pharmacology, School of Medicine, Loma Linda University, 11041 Campus Street, Loma Linda, CA 92354, USA. [4]Department of Neurosurgery, School of Medicine, Loma Linda University, 11234 Anderson Street, Loma Linda, CA 92354, USA.

References
1. Ballabh P, de Vries L. White matter injury in infants with intraventricular haemorrhage: mechanisms and therapies. Nat Rev Neurol. 2021;17:199–214.
2. Hierro-Bujalance C, Infante-Garcia C, Sanchez-Sotano D, Del Marco A, Casado-Revuelta A, Mengual-Gonzalez C, Lucena-Porras C, Bernal-Martin M, Benavente-Fernandez I, Lubian-Lopez S, Garcia-Alloza M.

Erythropoietin improves atrophy, bleeding and cognition in the newborn intraventricular hemorrhage. Front Cell Dev Biol. 2020;8: 571258.

3. Holste K, Xia F, Ye F, Keep R, Xi G. Mechanisms of neuroinflammation in hydrocephalus after intraventricular hemorrhage: a review. Fluids Barriers CNS. 2022;19:28.

4. Ren H, Han R, Chen X, Liu X, Wan J, Wang L, Yang X, Wang J. Potential therapeutic targets for intracerebral hemorrhage-associated inflammation: an update. J Cereb Blood Flow Metab. 2020;40:1752–68.

5. Zhou Y, Wang Y, Wang J, Anne Stetler R, Yang Q. Inflammation in intracerebral hemorrhage: from mechanisms to clinical translation. Prog Neurobiol. 2014;115:25–44.

6. Wang T, Zhang J, Li P, Ding Y, Tang J, Chen G, Zhang J. NT-4 attenuates neuroinflammation via TrkB/PI3K/FoxO1 pathway after germinal matrix hemorrhage in neonatal rats. J Neuroinflamm. 2020;17:158.

7. Xu M, Seyler L, Bäuerle T, Kalinichenko L, Müller C, Huttner H, Schwab S, Manaenko A. Serelaxin activates eNOS, suppresses inflammation, attenuates developmental delay and improves cognitive functions of neonatal rats after germinal matrix hemorrhage. Sci Rep. 2020;10:8115.

8. Song J, Nilsson G, Xu Y, Zelco A, Rocha-Ferreira E, Wang Y, Zhang X, Zhang S, Ek J, Hagberg H, Zhu C, Wang X. Temporal brain transcriptome analysis reveals key pathological events after germinal matrix hemorrhage in neonatal rats. J Cereb Blood Flow Metab. 2022;42:1632–49.

9. Li P, Zhao G, Ding Y, Wang T, Flores J, Ocak U, Wu P, Zhang T, Mo J, Zhang J, Tang J. Rh-IFN-α attenuates neuroinflammation and improves neurological function by inhibiting NF-κB through JAK1-STAT1/TRAF3 pathway in an experimental GMH rat model. Brain Behav Immun. 2019;79:174–85.

10. Klebe D, McBride D, Flores J, Zhang J, Tang J. Modulating the immune response towards a neuroregenerative peri-injury milieu after cerebral hemorrhage. J Neuroimmune Pharmacol. 2015;10:576–86.

11. Fejes Z, Pócsi M, Takai J, Erdei J, Tóth A, Balogh E, Rusznyák Á, Fenyvesi F, Nagy A, Kappelmayer J, Jeney V, Nagy B Jr. Preterm intraventricular hemorrhage-induced inflammatory response in human choroid plexus epithelial cells. Int J Mol Sci. 2021;22:8648.

12. Rendevski V, Aleksovski B, Mihajlovska Rendevska A, Hadzi-Petrushev N, Manusheva N, Shuntov B, Gjorgoski I. Inflammatory and oxidative stress markers in intracerebral hemorrhage: relevance as prognostic markers for quantification of the edema volume. Brain Pathol. 2023;32:e13106.

13. Liu J, Li N, Zhu Z, Kiang K, Ng A, Dong C, Leung G. Vitamin D enhances hematoma clearance and neurologic recovery in intracerebral hemorrhage. Stroke. 2022;53:2058–68.

14. Aronowski J, Zhao X. Molecular pathophysiology of cerebral hemorrhage: secondary brain injury. Stroke. 2011;42:1781–6.

15. Easton A. Neutrophils and stroke - can neutrophils mitigate disease in the central nervous system? Int Immunopharmacol. 2013;17:1218–25.

16. Xiao L, Zheng H, Li J, Zeng M, He D, Liang J, Sun K, Luo Y, Li F, Ping B, et al. Targeting NLRP3 inflammasome modulates gut microbiota, attenuates corticospinal tract injury and ameliorates neurobehavioral deficits after intracerebral hemorrhage in mice. Biomed Pharmacother. 2022;149: 112797.

17. Ye B, Geng Z, Ma L, Geng J. Slit2 regulates attractive eosinophil and repulsive neutrophil chemotaxis through differential srGAP1 expression during lung inflammation. J Immunol (Baltimore, Md:1950). 2010;185:6294–305.

18. Legg J, Herbert J, Clissold P, Bicknell R. Slits and roundabouts in cancer, tumour angiogenesis and endothelial cell migration. Angiogenesis. 2008;11:13–21.

19. Nguemgo Kouam P, Rezniczek G, Kochanneck A, Priesch-Grzeszkowiak B, Hero T, Adamietz I, Bühler H. Robo1 and vimentin regulate radiation-induced motility of human glioblastoma cells. PLoS ONE. 2018;13: e0198508.

20. Kandilya D, Shyamasundar S, Singh D, Banik A, Hande M, Stünkel W, Chong Y, Dheen S. High glucose alters the DNA methylation pattern of neurodevelopment associated genes in human neural progenitor cells in vitro. Sci Rep. 2020;10:15676.

21. Zhao H, Anand A, Ganju R. Slit2-Robo4 pathway modulates lipopolysaccharide-induced endothelial inflammation and its expression is dysregulated during endotoxemia. J Immunol (Baltimore, Md:1950). 2014;192:385–93.

22. Liu J, Liu H, Chen L. The therapeutic role of Slit2 in anti-fibrosis, anti-inflammation and anti-oxidative stress in rats with coronary heart disease. Cardiovasc Toxicol. 2021;21:973–83.

23. London N, Zhu W, Bozza F, Smith M, Greif D, Sorensen L, Chen L, Kaminoh Y, Chan A, Passi S, et al. Targeting Robo4-dependent Slit signaling to survive the cytokine storm in sepsis and influenza. Sci Transl Med. 2010;2:23ra19.

24. Altay T, McLaughlin B, Wu J, Park T, Gidday J. Slit modulates cerebrovascular inflammation and mediates neuroprotection against global cerebral ischemia. Exp Neurol. 2007;207:186–94.

25. Kaur H, Xu N, Doycheva D, Malaguit J, Tang J, Zhang J. Recombinant Slit2 attenuates neuronal apoptosis via the Robo1-srGAP1 pathway in a rat model of neonatal HIE. Neuropharmacology. 2019;158: 107727.

26. Sherchan P, Huang L, Wang Y, Akyol O, Tang J, Zhang J. Recombinant Slit2 attenuates neuroinflammation after surgical brain injury by inhibiting peripheral immune cell infiltration via Robo1-srGAP1 pathway in a rat model. Neurobiol Dis. 2016;85:164–73.

27. Yeh M, Gonda Y, Mommersteeg M, Barber M, Ypsilanti A, Hanashima C, Parnavelas J, Andrews W. Robo1 modulates proliferation and neurogenesis in the developing neocortex. J Neurosci. 2014;34:5717–31.

28. Pilling D, Chinea L, Consalvo K, Gomer R. Different isoforms of the neuronal guidance molecule Slit2 directly cause chemoattraction or chemorepulsion of human neutrophils. J Immunol (Baltimore, Md:1950). 2019;202:239–48.

29. Zamboni V, Jones R, Umbach A, Ammoni A, Passafaro M, Hirsch E, Merlo G. Rho GTPases in intellectual disability: from genetics to therapeutic opportunities. Int J Mol Sci. 2018;19:821.

30. Prasad A, Qamri Z, Wu J, Ganju R. Slit-2/Robo-1 modulates the CXCL12/CXCR4-induced chemotaxis of T cells. J Leukoc Biol. 2007;82:465–76.

31. Lekic T, Manaenko A, Rolland W, Krafft P, Peters R, Hartman R, Altay O, Tang J, Zhang J. Rodent neonatal germinal matrix hemorrhage mimics the human brain injury, neurological consequences, and post-hemorrhagic hydrocephalus. Exp Neurol. 2012;236:69–78.

32. Washington P, Lee C, Dwyer M, Konofagou E, Kernie S, Morrison B. Hyaluronidase reduced edema after experimental traumatic brain injury. J Cereb Blood Flow Metab. 2020;40:2026–37.

33. Yiin J, Hu B, Jarzynka M, Feng H, Liu K, Wu J, Ma H, Cheng S. Slit2 inhibits glioma cell invasion in the brain by suppression of Cdc42 activity. Neuro Oncol. 2009;11:779–89.

34. Moulin T, Ferro F, Hoyer A, Cheung P, Williams M, Schiöth H. Drosophila melanogaster the levodopa-induced depression model exhibits negative geotaxis deficits and differential gene expression in males and females. Front Neurosci. 2021;15: 653470.

35. Gao S, Calderon D. Robust alternative to the righting reflex to assess arousal in rodents. Sci Rep. 2020;10:20280.

36. Thullier F, Lalonde R, Cousin X, Lestienne F. Neurobehavioral evaluation of lurcher mutant mice during ontogeny. Brain Res Dev Brain Res. 1997;100:22–8.

37. Deacon RMJ. Measuring motor coordination in mice. J Vis Exp JoVE. 2013;75:e2609.

38. Göhrig A, Detjen K, Hilfenhaus G, Körner J, Welzel M, Arsenic R, Schmuck R, Bahra M, Wu J, Wiedenmann B, Fischer C. Axon guidance factor SLIT2 inhibits neural invasion and metastasis in pancreatic cancer. Can Res. 2014;74:1529–40.

39. Terzi A, Roeder H, Weaver C, Suter D. Neuronal NADPH oxidase 2 regulates growth cone guidance downstream of slit2/robo2. Dev Neurobiol. 2021;81:3–21.

40. Liu J, Hou W, Guan T, Tang L, Zhu X, Li Y, Hou S, Zhang J, Chen H, Huang Y. Slit2/Robo1 signaling is involved in angiogenesis of glomerular endothelial cells exposed to a diabetic-like environment. Angiogenesis. 2018;21:237–49.

41. Tole S, Mukovozov I, Huang Y, Magalhaes M, Yan M, Crow M, Liu G, Sun C, Durocher Y, Glogauer M, Robinson L. The axonal repellent, Slit2, inhibits directional migration of circulating neutrophils. J Leukoc Biol. 2009;86:1403–15.

42. Chaturvedi S, Robinson L. Slit2-Robo signaling in inflammation and kidney injury. Pediatr Nephrol (Berlin, Germany). 2015;30:561–6.

43. Minocha S, Valloton D, Ypsilanti A, Fiumelli H, Allen E, Yanagawa Y, Marin O, Chédotal A, Hornung J, Lebrand C. Nkx2.1-derived astrocytes and neurons together with Slit2 are indispensable for anterior commissure formation. Nat Commun. 2015;6:6887.

44. Zakrys L, Ward R, Pediani J, Godin A, Graham G, Milligan G. Roundabout 1 exists predominantly as a basal dimeric complex and this is unaffected by binding of the ligand Slit2. Biochem J. 2014;461:61–73.

Li *et al. Journal of Neuroinflammation*   (2023) 20:249

Page 16 of 16

45. Gangaraju S, Sultan K, Whitehead S, Nilchi L, Slinn J, Li X, Hou S. Cerebral endothelial expression of Robo1 affects brain infiltration of polymorphonuclear neutrophils during mouse stroke recovery. Neurobiol Dis. 2013;54:24–31.

46. Appe A, Aggerholm A, Hansen M, Ebbesen L, Hokland P, Bentzen H, Nyvold C. Differential expression levels and methylation status of ROBO1 in mantle cell lymphoma and chronic lymphocytic leukaemia. Int J Lab Hematol. 2017;39:e70–3.

47. Yuen D, Huang Y, Liu G, Patel S, Fang F, Zhou J, Thai K, Sidiqi A, Szeto S, Chan L, et al. Recombinant N-terminal Slit2 inhibits TGF-β-induced fibroblast activation and renal fibrosis. J Am Soc Nephrol. 2016;27:2609–15.

48. Anrather J, Iadecola C. Inflammation and stroke: an overview. Neurotherapeutics. 2016;13:661–70.

49. Huang X, Hussain B, Chang J. Peripheral inflammation and blood-brain barrier disruption: effects and mechanisms. CNS Neurosci Ther. 2021;27:36–47.

50. Chen Q, Zhou X, Hou R, Zhou Z, Wang Z, Chen Y, Weng J, Xu J. Aminophylline modulates the permeability of endothelial cells via the Slit2-Robo4 pathway in lipopolysaccharide-induced inflammation. Exp Ther Med. 2021;22:1042.

51. Weng J, Zhou X, Xie H, Gao Y, Wang Z, Gong Y. Slit2/Robo4 signaling pathway modulates endothelial hyper-permeability in a two-event in vitro model of transfusion-related acute lung injury. Blood Cells Mol Dis. 2019;76:7–12.

52. Sherchan P, Travis Z, Tang J, Zhang J. The potential of Slit2 as a therapeutic target for central nervous system disorders. Expert Opin Ther Targets. 2020;24:805–18.

53. Sas A, Carbajal K, Jerome A, Menon R, Yoon C, Kalinski A, Giger R, Segal B. A new neutrophil subset promotes CNS neuron survival and axon regeneration. Nat Immunol. 2020;21:1496–505.

54. Xu P, Zhang X, Liu Q, Xie Y, Shi X, Chen J, Li Y, Guo H, Sun R, Hong Y, et al. Microglial TREM-1 receptor mediates neuroinflammatory injury via interaction with SYK in experimental ischemic stroke. Cell Death Dis. 2019;10:555.

55. Candelario-Jalil E, Dijkhuizen R, Magnus T. Neuroinflammation, stroke, blood–brain barrier dysfunction, and imaging modalities. Stroke. 2022;53:1473–86.

56. Dunaway C, Hwang Y, Lindsley C, Cook R, Wu J, Boothby M, Chen J, Brantley-Sieders D. Cooperative signaling between Slit2 and Ephrin-A1 regulates a balance between angiogenesis and angiostasis. Mol Cell Biol. 2011;31:404–16.

57. Qi C, Lan H, Ye J, Li W, Wei P, Yang Y, Guo S, Lan T, Li J, Zhang Q, et al. Slit2 promotes tumor growth and invasion in chemically induced skin carcinogenesis. Lab Investig. 2014;94:766–76.

58. Liu Y, Yin Z, Xu X, Liu C, Duan X, Song Q, Tuo Y, Wang C, Yang J, Yin S. Crosstalk between the activated Slit2-Robo1 pathway and TGF-β1 signalling promotes cardiac fibrosis. ESC Heart Fail. 2021;8:447–60.

59. Park S, Lee J, Lee S, Koh J, Kim B. SLIT2 inhibits osteoclastogenesis and bone resorption by suppression of Cdc42 activity. Biochem Biophys Res Commun. 2019;514:868–74.

Publisher's Note